

Wrinkling and Delamination of Thin Films on Compliant Substrates

Haixia Mei and Rui Huang*

Department of Aerospace Engineering and Engineering Mechanics, University of Texas, Austin, TX 78712, USA

* Corresponding author: ruihuang@mail.utexas.edu

Abstract When the surface of a soft material is coated with a stiff thin film, compression induced buckling instability of the thin film results in surface wrinkles, and wrinkling of the thin film may lead to fracture and delamination. In this work, cohesive interface elements are employed in finite element analysis to simulate progressive wrinkling and wrinkle-induced delamination of an elastic thin film on a compliant substrate. The critical strain for initiation of wrinkle-induced delamination compares closely with an analytical formula based on a strength criterion. Subsequent growth of the delamination crack depends on the interface toughness. Co-evolution of wrinkling and buckle-delamination is simulated using a sufficiently large model. The interaction between the two buckling modes is elucidated.

Keywords: Thin films, Wrinkling, Delamination

1. Introduction

Stiff thin films on compliant substrates are used in a wide range of technological applications, including flexible electronics [1], thin film metrology [2], and micro/nano-fabrication [3]. Similar material structures are abundant in nature [4]. The mechanical interaction between a stiff film and a compliant substrate leads to a rich variety of phenomena that either limit or inspire practical applications of the hybrid system integrating hard and soft materials. In particular, recent interests in micro/nano-scale thin film materials have exploited mechanical instability (buckling and wrinkling) as an enabling mechanism for novel applications. Mechanics of surface wrinkling has been studied extensively over the last decade [5-17]. While most of these studies have assumed perfect bonding between the film and the substrate, it has been occasionally pointed out that wrinkling may cause interfacial delamination [5, 18, 19]. On the other hand, interfacial delamination is a necessary condition for buckling of thin films attached to relatively stiff substrates [20-22]. Simultaneous buckling and delamination has also been observed in compressed thin films on compliant substrates [23-25]. Some experiments have shown both surface wrinkling and buckle-delamination co-existing in the same film/substrate system [18].

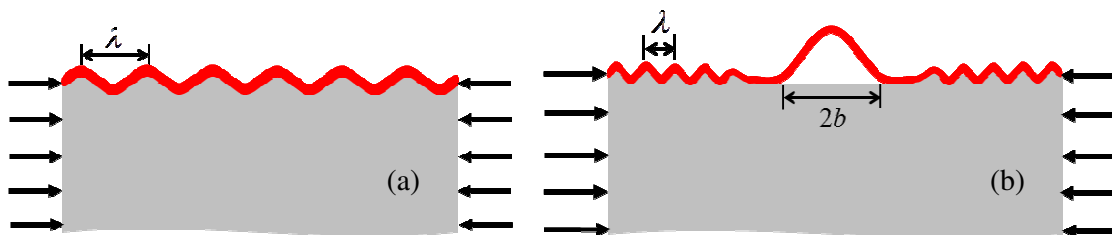


Figure 1. (a) wrinkling with no delamination; (b) Wrinkling and delamination.

In a previous work [18], we proposed a quantitative criterion for selection of the initial buckling mode by comparing the critical conditions for surface wrinkling and buckle delamination. The favored buckling mode at the onset of instability depends on the elastic mismatch between the film and the substrate as well as on the size of pre-existing interfacial delamination. More recently, by analytical and finite element methods, we presented a study on concomitant wrinkling and buckle-delamination for an elastic thin film on a highly compliant substrate [26]. In comparison with a nonlinear finite element analysis, an approximate formula was suggested to estimate the normal traction at the interface and to predict initiation of wrinkle-induced delamination. In this

paper, we present a study on nucleation and subsequent growth of wrinkle-induced delamination using a cohesive zone model.

2. Wrinkling Analysis

Consider an elastic thin film on an elastic compliant substrate, subject to lateral compression. Both the film and the substrate are taken to be linear elastic and isotropic, restricted to small, plane-strain deformation for the present study. Let ε be the nominal compressive strain, relative to the stress-free state. When ε is relatively small, the film/substrate bilayer is uniformly compressed and the surface is flat. When the strain exceeds a critical value, the film buckles and the substrate deforms coherently, forming surface wrinkles (Fig. 1a). The interface between the film and the substrate is assumed to be perfectly bonded in this section. Let h be the thickness of the film, while the substrate is considered infinitely thick. A well-known analytical solution predicts the critical strain for onset of wrinkling [9]:

$$\varepsilon_c = \frac{1}{4} \left(\frac{3\bar{E}_s}{\bar{E}_f} \right)^{2/3}, \quad (1)$$

where $\bar{E} = E/(1-\nu^2)$ is the plane-strain modulus with E for Young's modulus and ν for Poisson's ratio, and the subscripts f and s denote the film and substrate, respectively. The corresponding wrinkle wavelength is

$$\lambda = 2\pi h \left(\frac{\bar{E}_f}{3\bar{E}_s} \right)^{1/3}. \quad (2)$$

In deriving the above analytical solution, the shear traction at the film/substrate interface was assumed to be zero. Alternatively, by assuming zero tangential displacement at the interface, a similar analytical solution can be obtained [8, 13]. The two solutions are identical if the substrate is incompressible ($\nu_s = 0.5$), in which case both the shear traction and tangential displacement are zero. However, when the substrate is compressible ($\nu_s < 0.5$), neither the shear traction nor the tangential displacement is zero at the interface as the film wrinkles. As a result, neither analytical solution accurately accounts for the effect of Poisson's ratio of the substrate [15]. By taking into account both the shear traction and the tangential displacement at the interface, a more accurate analytical solution was developed [26], giving that

$$\varepsilon_c^* = \frac{1}{4} \left(\frac{3\bar{E}_s}{\bar{E}_f} \right)^{2/3} \left[1 - \frac{1}{4} \left(\frac{1-2\nu_s}{1-\nu_s} \right)^2 \right]^{-2/3}, \quad (3)$$

and

$$\lambda^* = 2\pi h \left(\frac{\bar{E}_f}{3\bar{E}_s} \right)^{1/3} \left[1 - \frac{1}{4} \left(\frac{1-2\nu_s}{1-\nu_s} \right)^2 \right]^{1/3}. \quad (4)$$

It was shown that, for a compressible substrate ($\nu_s < 0.5$), Eq. (1) underestimates the critical strain and Eq. (2) overestimates the wrinkle wavelength. The difference can be significant, up to about 20% for the critical strain and nearly 10% for the wavelength [26].

Beyond the critical strain, the wrinkle amplitude grows as a function of the nominal strain ε . An approximate solution for the wrinkle amplitude was obtained previously by a nonlinear approach that minimizes the strain energy in the film and the substrate [8, 9], namely

$$A = h \sqrt{\frac{\varepsilon}{\varepsilon_c} - 1}. \quad (5)$$

Finite element analysis (FEA) of wrinkling was performed using a two-dimensional (2D) plane-strain model in ABAQUS [26]. By a linear eigenvalue analysis, the finite element model predicted the critical strain for onset of wrinkling and the corresponding eigenmode, in good agreement with the analytical solutions in (3) and (4) when the substrate thickness is sufficiently large. To simulate wrinkle growth beyond the critical strain, a nonlinear post-buckling analysis was performed with the finite element model. Figure 2(a) shows the wrinkle amplitude as a function of the nominal strain for $E_f/E_s=1000$ and $\nu_f=\nu_s=1/3$. For comparison, the approximate analytical solution in (5) is plotted as a continuous solid line. The numerical results vary slightly as the amplitude of the initial imperfection (A_0/h) varies. Using a small initial imperfection ($A_0/h = 10^{-4}$), the numerical results compare closely with the analytical solution, with an abrupt transition at the critical strain. It is thus concluded that the analytical solution (5) is a good approximation for the wrinkle amplitude.

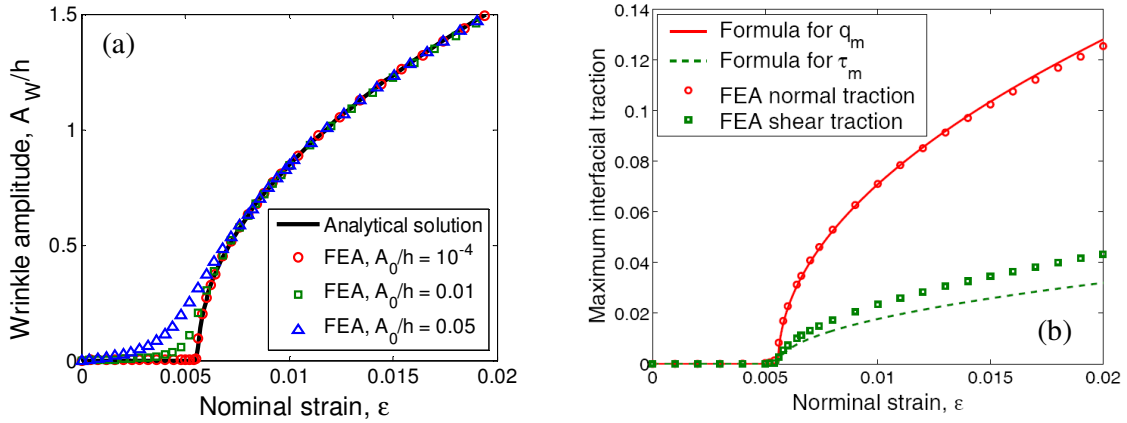


Figure 2. (a) wrinkle amplitude; (b) wrinkling-induced normal and shear tractions.

As the wrinkle amplitude grows, the normal and shear tractions acting on the film/substrate interface increase, which may cause delamination [5, 18, 19]. An approximate formula was derived to estimate the maximum normal traction at the interface [26]:

$$q_m = \frac{4(1-\nu_s)^2}{3-4\nu_s} \bar{E}_s \sqrt{\varepsilon - \varepsilon_c}. \quad (6)$$

The maximum shear traction is linearly related to the maximum normal traction, namely

$$\tau_m = \frac{1-2\nu_s}{2(1-\nu_s)} q_m. \quad (7)$$

By comparing to the FEA results, as shown in Fig. 2(b), it is found that the maximum normal traction by FEA follows (6) remarkably well, while the formula in (7) underestimates the maximum shear traction. The close agreement for the maximum normal traction suggests that the formula (6) may be used to estimate the critical strain for initiation of wrinkle-induced interfacial delamination. By setting the maximum normal traction equal the interfacial strength ($\hat{\sigma}_{int}$), the critical strain for initiation of wrinkle-induced delamination is obtained [26]:

$$\varepsilon_{WID} = \varepsilon_c + \left(\frac{3-4\nu_s}{4(1-\nu_s)^2} \frac{\hat{\sigma}_{int}}{\bar{E}_s} \right)^2. \quad (8)$$

where $\hat{\sigma}_{int}$ is the peak stress in the normal traction-separation relation for the interface as described by a cohesive zone model [27]. When $\varepsilon > \varepsilon_{WID}$, the interfacial delamination grows concomitantly with buckling (Fig. 1b).

3. Wrinkle-Induced Delamination

To simulate initiation and evolution of wrinkle-induced delamination, a two-dimensional finite element model was constructed in ABAQUS, as illustrated in Fig. 3(a). Both the film and the substrate were modeled by 2D quadrilateral elements (CPE8R). In addition, a layer of cohesive elements (COH2D4) was assigned along the interface to model the interaction between the film and the substrate. The bilinear traction-separation relation, as illustrated in Fig. 3(b), was used to describe the constitutive behavior of the cohesive elements.

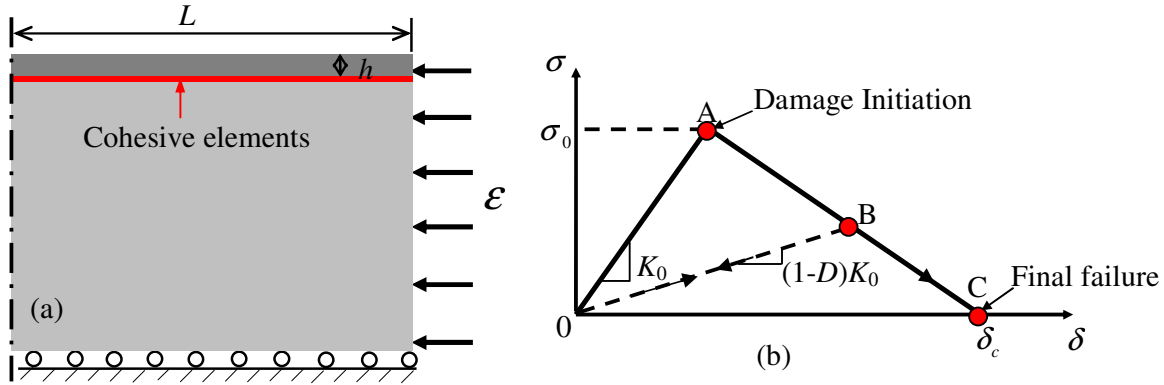


Figure 3. (a) Schematic illustration of the finite element model; (b) Illustration of the bilinear traction-separation law for the cohesive elements in ABAQUS.

A delamination crack along an interface is typically under a mixed-mode condition due to elastic mismatch between the film and the substrate [20]. Consequently, the interfacial properties are required for both modes I and II conditions. For the bilinear traction-separation model, the interfacial properties to be specified include [28]: the initial elastic stiffness K_n and K_s , the cohesive strength σ_n and τ_s , and the interface toughness Γ_I and Γ_{II} . In this section, we ignore the effect of mode mix by taking $K_n = K_s = K_0$, $\sigma_n = \tau_s = \sigma_0$ and $\Gamma_I = \Gamma_{II} = \Gamma$ for the interface. Previous studies have suggested that the initial elastic stiffness K_0 plays a less important role in cohesive zone modeling. In the present study, the initial stiffness K_0 is taken to be a constant (with $K_0 h / \bar{E}_f = 1$) in all simulations, while the strength (σ_0) and toughness (Γ) are varied. The elastic properties for the film and the substrate are such that $E_f/E_s = 1000$ and $\nu_f = \nu_s = 1/3$.

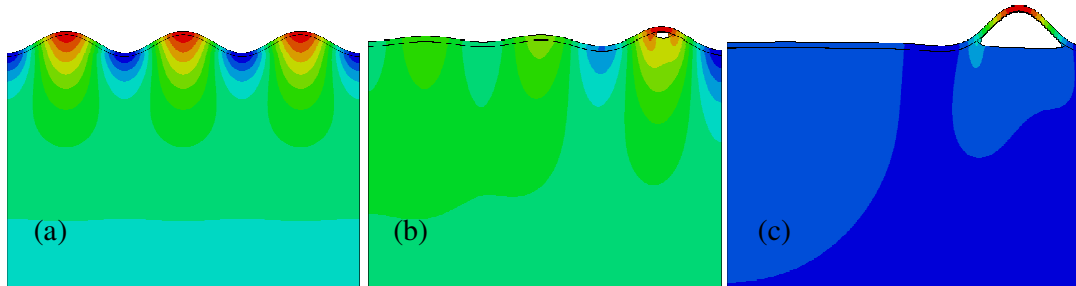


Figure 4. Numerical simulation of progressive wrinkling and interfacial delamination for an elastic thin film on a compliant substrate subject to increasing compression: (a) wrinkling with no delamination; (b) initiation of wrinkle-induced delamination; (c) subsequent growth of interfacial delamination.

Figure 4 shows an example of the numerical simulation. Start from an elastic film perfectly bonded to a compliant substrate (with a small initial perturbation). As the applied compressive strain increases, the film wrinkles first (Fig. 4a), followed by nucleation of an interfacial crack at one of the wrinkle crests (Fig. 4b). Upon subsequent growth of the delamination, buckling of the film becomes localized while the neighboring wrinkles are flattened (Fig. 4c).

In Section 2, initiation of wrinkle-induced delamination is predicted by comparing the maximum normal traction at the interface with the strength of the interface. This strength-based criterion for crack initiation is found to be in good agreement with the numerical results by the cohesive zone modeling approach. With the cohesive interface elements, a nonlinear post-buckling analysis is performed to simulate progressive wrinkling and wrinkle-induced delamination, as shown in Fig. 4. The amplitude of wrinkling or buckling is plotted as a function of the nominal strain in Fig. 5(a) for three different values of the interfacial strength, whereas the interfacial toughness is taken to be a constant, $\Gamma/\bar{E}_f h = 10^{-5}$. For comparison, the wrinkle amplitude without delamination is plotted as a continuous solid line. For each value of the interfacial strength, the wrinkle amplitude follows the solid line before the initiation of delamination. At a critical nominal strain that depends on the interfacial strength, a delamination crack is nucleated and the buckle amplitude at the location of delamination increases abruptly, deviating from the solid line. Thus, the initiation of delamination may be readily observable in experiments by measuring the buckle amplitude.

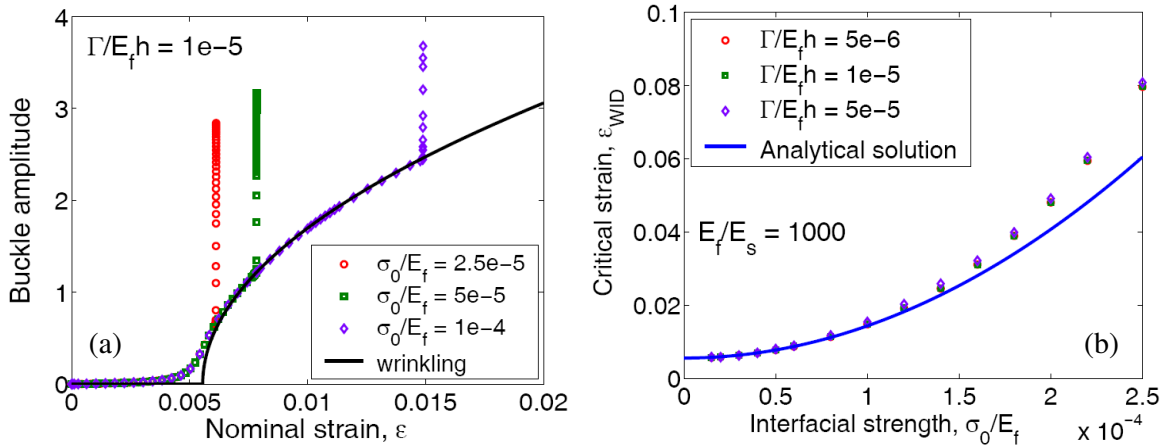


Figure 5. (a) Buckle amplitude as a function of the nominal strain, for three different values of interfacial strength. The solid line represents the wrinkle amplitude by the analytical solution in Eq. (5). (b) The critical strain for initiation of wrinkle-induced delamination as a function of the interfacial strength.

The critical strain for initiation of wrinkle-induced delamination can be determined from Fig. 5(a). Alternatively, by the cohesive zone model, each cohesive element is characterized by a damage parameter (D), which varies between 0 and 1 during the separation process [28]. Thus, the critical strain for crack nucleation can be determined numerically when the damage parameter reaches 1 for at least one of the cohesive elements. Figure 5(b) plots the critical strain for wrinkle-induced delamination as a function of the interfacial strength, for three different values of interface toughness. For comparison, the critical strain predicted by the analytical formula in Eq. (8) is plotted as the solid line. Clearly, the critical strain is nearly independent of the interface toughness, justifying the strength-based criterion. The numerical results agree closely with the analytical prediction for relatively low interfacial strengths (e.g., $\sigma_0/\bar{E}_f < 10^{-4}$). For higher interfacial strengths, however, Eq. (8) underestimates the critical strain. Apparently, since the critical strain increases with increasing interfacial strength, the linear approximation of the normal traction that leads to Eq. (8) becomes increasingly inaccurate as the strain goes beyond a few per cent.

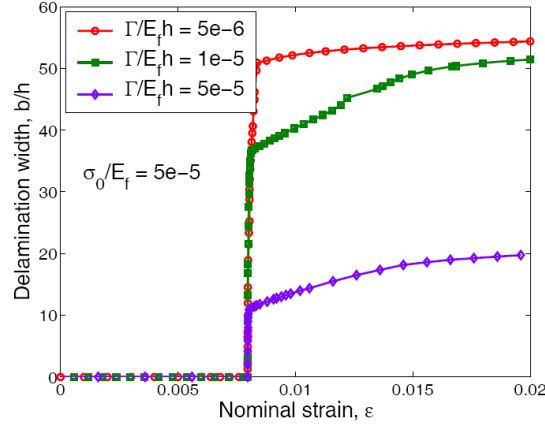


Figure 6. Delamination width as a function of the nominal strain for different values of interface toughness.

While the initiation of wrinkle-induced delamination is independent of the interface toughness, subsequent growth of the delamination crack does depend on the interface toughness. As shown in Figure 6, for an interfacial strength $\sigma_0/\bar{E}_f = 5 \times 10^{-5}$, the delamination width (b) as a function of the nominal strain is plotted for three different values of interface toughness. The delamination width is determined from the cohesive zone model based on the damage parameters of the cohesive elements. The delamination width remains zero until the critical strain is reached. Upon initiation, the delamination crack grows rapidly, which in turn leads to rapid growth of the buckle amplitude as shown in Fig. 5(a). The growth of the interfacial crack is eventually stabilized with a delamination width depending on the interface toughness. Further increasing the compressive strain, the delamination grows stably. Apparently, under the same nominal strain (greater than the critical strain), the delamination width decreases as the interface toughness increases.

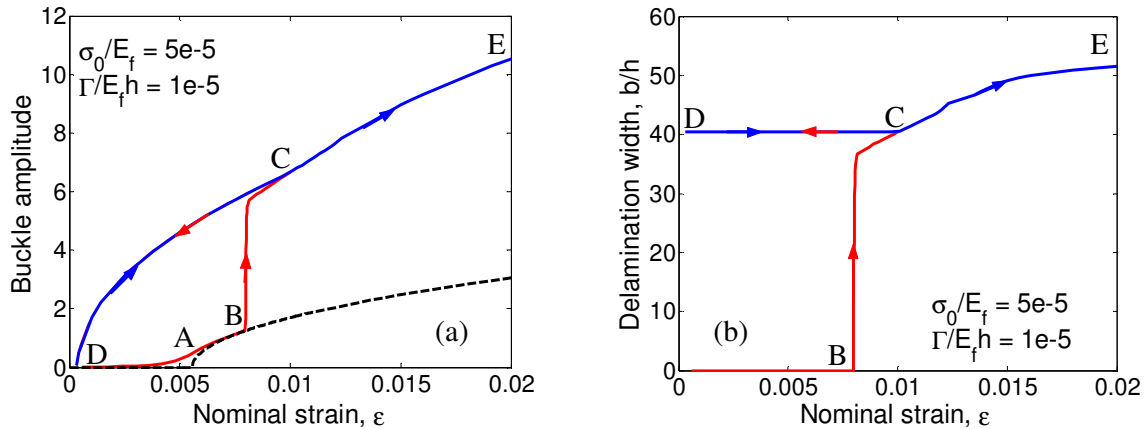


Figure 7. (a) Buckle amplitude and (b) delamination width as a function of the nominal strain during a loading-unloading-reloading cycle.

The cohesive zone elements as implemented in ABAQUS assume an irreversible damage process, which may be used to simulate damage accumulation under cyclic loading. As an example, numerical simulation of a loading-unloading-reloading process is performed, with $\sigma_0/\bar{E}_f = 5 \times 10^{-5}$ and $\Gamma/\bar{E}_f h = 10^{-5}$. Figure 7(a) shows the buckle amplitude versus the nominal strain. Before the first loading, the interface is perfectly bonded with no damage ($D = 0$). As the nominal strain increases, wrinkling occurs first at point A ($\varepsilon \sim 0.00556$), and wrinkle-induced delamination initiates at B ($\varepsilon \sim 0.0076$). Subsequently, delamination and buckling co-evolve. The corresponding delamination width is shown in Fig. 7(b). Start unloading at point C ($\varepsilon = 0.01$). The delamination

width remains a constant ($b/h \sim 40$) during unloading. Meanwhile, the buckle amplitude decreases, following a different path from C to D. The buckle amplitude is nearly zero at D, with the nominal strain ($\varepsilon \sim 0.000384$) corresponding to the critical strain for onset of buckling with $b/h \sim 40$. Upon reloading, the buckle amplitude follows the same path of unloading from D to C, during which the delamination does not grow. Further increasing the nominal strain beyond C to point E ($\varepsilon = 0.02$), the delamination grows and the buckle amplitude increases. Apparently, the buckle amplitude during reloading follows a drastically different path compared to that for the first loading. Such a behavior qualitatively agrees with an experiment by Vella et al. [25]. However, in their experiment, a discontinuous jump of the buckle amplitude during the first loading was reported, presumably due to the unstable growth of the delamination.

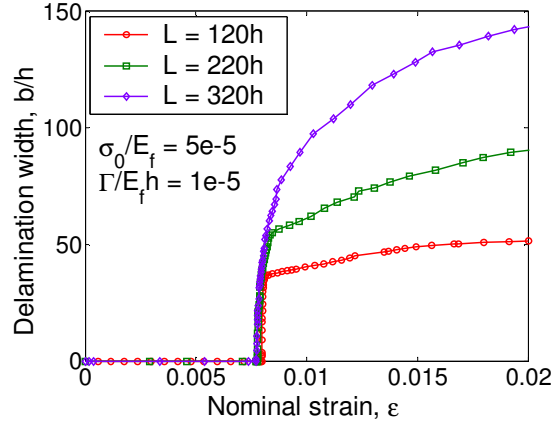


Figure 8. Delamination width as a function of the nominal strain for different lengths used in the finite element model.

It is noted that the growth of buckle-delamination is strongly influenced by the boundary condition. When the crack tip approaches one end of the model, where the symmetric boundary condition is assumed, the energy release rate drops rapidly and the crack is arrested when the energy release rate is less than the interface toughness. Figure 8 shows the delamination width as a function of the nominal strain by finite element models with three different lengths (L). Apparently, as L increases, the delamination width increases upon initiation, while the critical strain for initiation is insensitive to the model size.

With a sufficiently large L/b , the localized buckle-delamination and periodic wrinkles may co-exist [26]. To simulate both initiation and co-evolution of wrinkling and buckle-delamination, the finite element model with cohesive elements is employed with $L = 1000h$ and $H = 200h$. The bilinear traction-separation relation is assumed for the interface with $\sigma_0/\bar{E}_f = 5 \times 10^{-5}$ and $\Gamma/\bar{E}_f h = 5 \times 10^{-5}$. Figure 9 shows the evolution of deformation profiles of the film (solid lines) and the substrate surface (dashed lines) with increasing nominal strain. The film remains flat until the nominal strain reaches the critical strain for wrinkling ($\varepsilon_w = 0.00556$). Beyond the critical strain, periodic wrinkles form as shown in Fig. 9(a) at $\varepsilon = 0.00758$. As the nominal strain increases to the critical value for wrinkle-induced delamination ($\varepsilon_{wid} = 0.0076$), an interfacial crack initiates and grows rapidly, as shown in Figs. 9 (b) and (c) for two strains slightly above the critical strain. The growth of delamination leads to large, localized buckling, which relaxes the compressive stress in the film over a region close to the delamination. As a result, the wrinkles are flattened in the relaxation region. Further away from the delamination, the film remains wrinkled. The size of the relaxation region depends on the relative compliance of the substrate and the delamination width. With continuous growth of the delamination and a finite length ($L = 1000h$) in the finite element model, all the wrinkles are flattened eventually, as shown in Fig. 9(d).

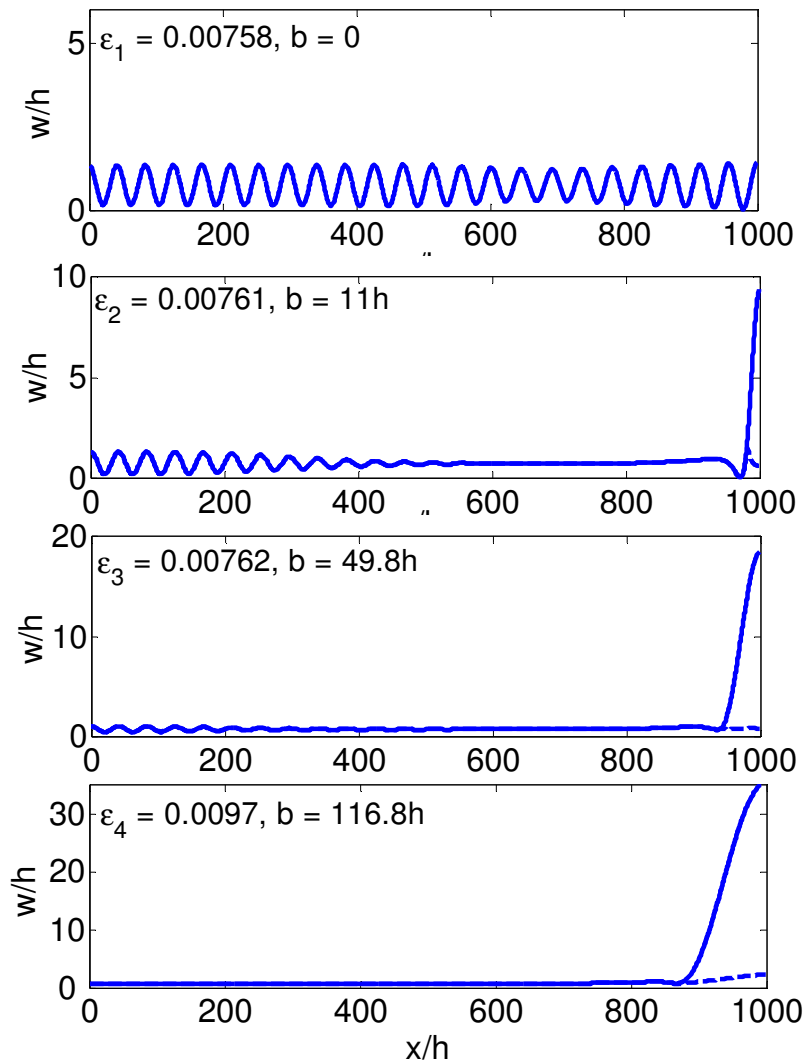


Figure 9. Out-of-plane displacement of the film (solid lines) and the substrate surface (dashed lines) at four different nominal strains: (a) $\varepsilon = 0.00758$; (b) $\varepsilon = 0.00761$ ($b = 11h$); (c) $\varepsilon = 0.00762$ ($b = 49.8h$); (d) $\varepsilon = 0.0097$ ($b = 116.8h$).

4. Summary

Cohesive interface elements are employed in finite element analysis to simulate initiation and growth of wrinkle-induced delamination of an elastic thin film on a compliant substrate. The critical strain for initiation of wrinkle-induced delamination compares closely with an analytical formula based on a strength criterion. Subsequent growth of the delamination crack depends on the interface toughness. Co-evolution of wrinkling and buckle-delamination is simulated using a sufficiently large model. The interaction between the two buckling modes is elucidated.

Acknowledgements

This work was supported by Semiconductor Research Corporation (SRC).

References

1. Rogers, J.A., Someya, T., Huang, Y., 2010. Materials and Mechanics for Stretchable Electronics. Science 327, 1603-1607.
2. Chung, J. Y., Nolte, A.J., Stafford, C.M., 2011. Surface wrinkling: a versatile platform for measuring thin-film properties. Advanced Materials 23, 349-368.

3. Bowden, N., Brittain, S., Evans, A.G., Hutchinson, J.W., and Whitesides, G.M., 1998. Spontaneous formation of ordered structures in thin films of metals supported on an elastomeric polymer. *Nature* 393, 146-149.
4. Chen, X., and Yin, J., 2010. Buckling patterns of thin films on curved compliant substrates with applications to morphogenesis and three-dimensional micro-fabrication. *Soft Matter* 6, 5667-5680.
5. Shield, T.W., Kim, K.-S., Shield, R.T., 1994. The buckling of an elastic layer bonded to an elastic substrate in plane strain. *J. Appl. Mech.* 61, 231-235.
6. Huang, R., and Suo, Z., 2002. Instability of a compressed elastic film on a viscous layer. *International Journal of Solids and Structures* 39, 1791-1802.
7. Chen, X., and Hutchinson, J.W., 2004. Herringbone buckling patterns of compressed thin films on compliant substrates. *J. Appl. Mech.* 71, 597-603.
8. Huang, R., 2005. Kinetic wrinkling of an elastic film on a viscoelastic substrate. *J. Mech. Phys. Solids* 53, 63-89.
9. Huang, Z.Y., Hong, W., and Suo, Z., 2005. Nonlinear analysis of wrinkling in a film bonded to a compliant substrate. *J. Mech. Phys. Solids* 53, 2101-2118.
10. Huang, R., and Im, S.H., 2006. Dynamics of wrinkle growth and coarsening in stressed thin films. *Physical Review E* 74, 026214.
11. Jiang, H.Q., Khang, D.-Y., Song, J., Sun, Y., Huang, Y., Rogers, J.A., 2007. Finite deformation mechanics in buckled thin films on compliant supports. *Proc. Natl. Acad. Sci.* 104, 15607–15612.
12. Lee, D., Triantafyllidis, N., Barbar, J.R., Thouless, M.D., 2008. Surface instability of an elastic half space with material properties varying with depth. *J. Mech. Phys. Solids* 56, 858-868.
13. Audoly, B., and Boudaoud, A., 2008. Buckling of a stiff film bound to a compliant substrate. Part I: formulation, linear stability of cylindrical patterns, secondary bifurcations. *J. Mech. Phys. Solids* 56, 2401-2421.
14. Im, S.H., and Huang, R., 2008. Wrinkle Patterns of Anisotropic Crystal Films on Viscoelastic Substrates. *J. Mech. Phys. Solids* 56, 3315-3330.
15. Cai, S., Breid, D., Crosby, A. J., Suo, Z., Hutchinson, J. W., 2011. Periodic patterns and energy states of buckled films on compliant substrates. *J. Mech. Phys. Solids* 59, 1094–1114.
16. Sun, J.-Y., Xia, S., Moon, M.-W., Oh, K. H., Kim, K.-S., 2012. Folding wrinkles of a thin stiff layer on a soft substrate. *Proc. R. Soc. A* 468, 932–953.
17. Cao, Y., Hutchinson, J.W., 2012. Wrinkling phenomena in Neo-Hookean film/substrate bilayers. *J. Appl. Mech.* 79, 031019.
18. Mei, H., Huang, R., Chung, J.Y., Stafford, C.M., Yu, H.H., 2007. Buckling modes of elastic thin films on elastic substrates. *Appl. Phys. Lett.* 90, 151902.
19. Goyal, S., Srinivasan, K., Subbarayan, G., Siegmund, T., 2010. On instability-induced debond initiation in thin film systems. *Eng. Fracture Mechanics* 77, 1298-1313.
20. Hutchinson, J.W., and Suo, Z., 1992. Mixed-mode cracking in layered materials. *Adv. Appl. Mech.* 29, 63-191.
21. Ortiz, M., and Gioia, G., 1997. Delamination of compressed thin films. *Adv. Appl. Mech.* 33, 119-192.
22. Moon, M.-W., Chung, J.-W., Lee, K.-R., Oh, K.H., Wang, R., Evans, A.G., 2002. An experimental study of the influence of imperfections on the buckling of compressed thin films. *Acta Mater.* 50, 1219-1227.
23. Cotterell, B., and Chen, Z., 2000. Buckling and cracking of thin films on compliant substrates under compression. *Int. J. Fracture* 104, 169-179.
24. Parry, G., Colin, J., Coupeau, C., Foucher, F., Cimetiere, A., Grilhe, J., 2005. Effect of substrate compliance on the global unilateral post-buckling of coatings: AFM observations and finite element calculations. *Acta Mater.* 53, 441-447.
25. Vella, D., Bico, J., Boudaoud, A., Roman, B., Reis, P.M., 2009. The macroscopic delamination of thin films from elastic substrates. *PNAS* 106, 10901-10906.
26. Mei, H., Landis, C.M., Huang, R., 2011. Concomitant wrinkling and buckle-delamination of elastic thin films on compliant substrates. *Mechanics of Materials* 43, 627-642.
27. Hutchinson, J.W., and Evans, A.G., 2000. *Mechanics of Materials: Top down approaches to fracture.* *Acta Mater.* 48, 125-135.
28. Mei, H., Gowrishankar, S., Liechti, K. M., Huang, R., 2010. Initiation and propagation of interfacial delamination in integrated thin-film structures. *Proc. 12th IEEE Intersociety Conference on Thermal and Thermomechanical Phenomena in Electronic Systems (ITherm), Las Vegas, NV, June 2010.*